Dynamical classic limit. Dissipative vs. conservative systems

G. Gonzalez Acosta,[1] A. Plastino,[1] and A.M. Kowalski[1, a)]
Instituto de Físusica (IFLP-CCT-Conicet), Fac. de Ciencias Exactas, Universidad Nacional de La Plata, 1900 La Plata, Argentina

(Dated: 6 December 2022)

We analyze the nonlinear dynamics of a quartic semiclassical system able to describe the interaction of matter with a field. We do it both in a dissipative and a conservative scenarios. In particular, we study the classical limit of both frameworks and compare the associated features. In the two environments we heavily use a system's invariant, related to the Uncertainty Principle, that helps to determine how the dynamics tends to the pertinent classical limit. We exhibit the convergence to the classical limit and also verify that the Uncertainty Principle is complied with during the entire process, even in the presence of dissipation.

The transition between the microscopic world described by quantum mechanics and the macroscopic world explained by classical mechanics is a frontier issue in physics. A widely accepted view of the issue appeals to the idea of decoherence. The entanglement of a quantum system disappears due to interaction with the environment. A subtopic of the decoherence view is the classic Limit of Quantum Dynamics (LC). We use a semi-quantum methodology in which quantum and classical degrees of freedom interact. This approximation can be adopted when the quantum effects of one of the systems are small enough. For example, when a quantum system interacts with a macroscopic system in a measurement process. In our picture, a simple non linear set of equations arises that we solve using orthodox methods. Using this methodology, no quantum rules of the sub-quantal system are violated,

We study the LC by varying a relative energy related to the Uncertainty Principle and comparing the semiclassical dynamics with that of its classical analog. We have analyzed several semiclassical systems, finding interesting traits and that the classical limit does exist. . Our goal is to verify if these features are of a general nature, which would constitute an interesting contribution to the knowledge of Quantum Dynamics. Therefore, we analyze systems with markedly different characteristics, in order to understand and obtain an overall picture. In this work we consider a system never studied before, whose dynamics is regular. In previous studies of other systems we found chaos. In addition, we will analyze here, for the first time, the dissipative regime. To evaluate the LC transition we calculate 1) a series of Poincare Sections in the conservative case and 2) three-dimensional Poincare Sections and their projections in the dissipative instance. We find that the LC exists and that the common properties mentioned above hold.

[a)]Corresponding author: A.M. Kowalski; kowalski@fisica.unlp.edu.ar

I. INTRODUCTION

The quantum-classical transition (QCT) is certainly a frontier issue that constitutes an important physics topic[1–5]. The QCT is related to the use of semi-classical systems to describe special problems. This is an issue with a long history[6–12]. A particularly important case is to be highlighted: that in which quantum features in one of the two components of a bipartite system are negligible in comparison to the other. Regarding this scenario as semi classical simplifies the description and provides deep insight into the combined system dynamics[13]. This methodology is widely used for the interaction of matter with a field. In previous efforts we looked at these matters through a well-known conservative model[14,15] and to its totally classic counterpart. We always encounter chaos in such counterpart. Here we look at a different Hamiltonian (semi and totally classic versions). We study the regular regimes of the system in its conservative version and also in the presence of dissipation[18–20], and try to understand the QCT.

Motivation We have in the past analyzed several semiclassical systems, finding notable properties (for instance that the classical limit does exist) in Refs. 15, 18, and 19. This motivates us to try to ascertain whether the features there encountered are of a general character, which would constitute an interesting contribution to the knowledge of Quantum Dynamics. Therefore, we analyze systems with markedly different characteristics to that of 15, 18, and 19, in order get an overall dynamical picture. Accordingly, we work with a system never studied before. In the present system the dynamics is regular while in Ref. 15 we found chaos. In addition, we analyze for the first time the classical limit of a dissipative regime. To evaluate the transition to classicality we calculate a series of Poincare Sections in the conservative case and three-dimensional Poincare Sections (together with their Projections) in the dissipative instance. We will find that the classical limit exists and that the notable properties alluded to above still hold.

The paper is organized as follows: in Sect. II we describe the model to be analyzed and review its main features. Some interesting analytic and numerical results are presented in Section III. We analyze the conservative regime in Sub-Section III A and the dissipative evolution in Sub-Section III B. Finally,

some conclusions are drawn in Sect. IV.

II. MODEL

Our Hamiltonian reads

$$\hat{H} = \frac{1}{2}\left(\omega_q\left(\hat{x}^2+\hat{p}^2\right)+\omega_{cl}\left(A^2+P_A^2\right)\hat{I}+e_q^{cl}A^2\hat{x}^2\right), \quad (1)$$

where $\hat{x}$ and $\hat{p}$ are quantum operators while A and P_A are canonically conjugated classic variables. $\hat{I}$ is the Identity operator. This Hamiltonian depicts the interaction between a quantum and a classical oscillators. The interaction is represented by means of a quartic term dependent on both types of variables. This Hamiltonian can describe the interaction between the interaction of matter with a field.

Variables with "natural" dimensionality are recast in (1). How? Via $\hat{x}^d = \hat{x}/\sqrt{m_q\omega_q}$ and $\hat{p}^d = \sqrt{m_q\omega_q}\,\hat{p}$. These transforms simplify the dependence on the parameters and leave untouched the commutation relations. A similar change is made for the classical variables. Accordingly, all variables in (1) have units of an action's square root. ω_q and ω_{cl} are frequencies and e_q^{cl} a parameter positive. The time evolution of our operators is the canonical one. Note, however, that the Hamiltonian depends upon the classical variables A and P_A. These classical quantities obey Hamilton's equations, of course, where the temporal generator is the mean value of the Hamiltonian[14,15]. If we add to the Hamiltonian an appropriate ad hoc term we get dissipation[18–20].
Thus, for a given operator we have

$$\frac{d\hat{O}}{dt} = \frac{i}{\hbar}\left[\hat{H},\hat{O}\right]. \quad (2)$$

The evolution of $\langle\hat{O}\rangle \equiv \mathrm{Tr}\left[\rho\hat{O}(t)\right]$ is provided by

$$\frac{d\langle\hat{O}\rangle}{dt} = \frac{i}{\hbar}\left\langle\left[\hat{H},\hat{O}\right]\right\rangle, \quad (3)$$

using a suitable density operator $\rho(0)$.
$[\hat{H},\hat{O}_i]$ can always be cast as[16,17]

$$[\hat{H},\hat{O}_i] = i\hbar\sum_{j=1}^{q} g_{ji}\hat{O}_j\,, \qquad i=0,1,\ldots,q, \quad (4)$$

where we can have $q\to\infty$. We are interested in finite q-values. In this case it is said that the set of operators $\hat{O}_i$, $i=0,1,\ldots,q$, close a Lie semialgebra with $\hat{H}$[16,17]. For a semiclassical Hamiltonian like (1), the coefficients g_{ji} depend on A and P_A. For classical variables one

$$\frac{dA}{dt} = \frac{\partial\langle\hat{H}\rangle}{\partial P_A}, \quad (5a)$$

$$\frac{dP_A}{dt} = -\frac{\partial\langle\hat{H}\rangle}{\partial A} - \eta P_A, \quad (5b)$$

where if $\eta > 0$ our system is dissipative. Instead, if $\eta = 0$, it is conservative.
To verify these features[18–20] a particularly convenient space is used. We will call it "v-space". With respect to it, a bunch of equations deduced from Eqs. (3) and (5) conform an autonomous set of equations. They are first-order coupled differential ones, of the type[18–20]

$$\frac{d\vec{v}}{dt} = \vec{F}(\vec{v}), \quad (6)$$

with $\vec{v}$ is a "vector". It is regarded as a variable containing both classical and quantum parts. We consider volume elements V_S of this space, surrounded by a surface S. The dissipative η term generates a contraction of V_S[22]. The divergence of our vector is seen to be $-\eta$, given the fact that the matrix G in equations (4) is traceless. This happens due to the canonical character of Eqs. (2). Consequently. we must have[18–20]

$$\frac{dV_S(t)}{dt} = -\eta V_S(t). \quad (7)$$

Accordingly, we deal with a dissipative system[22]. If the classical Hamiltonian is of the form

$$H_{cl} = \frac{1}{2M}P_A^2 + V(A), \quad (8)$$

then the time-evolution of the total energy $\langle\hat{H}\rangle$ becomes (see Appendix A)

$$\frac{d\langle\hat{H}\rangle}{dt} = -\frac{\eta}{M}P_A^2. \quad (9)$$

Its meaning is to be ascertained through the lens of Eq. (7)[18–20]
The complete set of equations (3) + (5) constitutes an autonomous set of non-linear coupled first-order ordinary differential equations (ODE). They allow for a dynamical description in which no quantum rules of the sub-quantal system are violated, e.g-, the commutation-relations are trivially conserved at all times, since the quantum evolution is the canonical one for an effective time-dependent Hamiltonian (A and P_A, play the role of time-dependent parameters of the quantum system). The initial conditions are determined by a suitable quantum density operator $\hat{\rho}$. This happens both in the dissipative and in the conservative instances[13,20].

A. Equations of motion and classical limit

For Eqs. (3) we appeal to the set $(\hat{x}^2,\hat{p}^2,\hat{L}=\hat{x}\hat{p}+\hat{x}\hat{p})$. This is the minimum one that encompasses the uncertainty inequalities (see below the relevant Eq. 14). Thus,

$$\frac{d\langle\hat{x}^2\rangle}{dt} = \omega_q\langle\hat{L}\rangle, \quad (10a)$$

$$\frac{d\langle\hat{p}^2\rangle}{dt} = -\left(\omega_q + e_q^{cl}A^2\right)\langle\hat{L}\rangle, \quad (10b)$$

$$\frac{d\langle\hat{L}\rangle}{dt} = 2\left(\omega_q\langle\hat{p}^2\rangle - \left(\omega_q + e_q^{cl}A^2\right)\langle\hat{x}^2\rangle\right). \quad (10c)$$

For the classical variables we have

$$\frac{dA}{dt} = \omega_{cl} P_A, \tag{11a}$$

$$\frac{dP_A}{dt} = -A\left(\omega_{cl} + e_q^{cl}\left\langle \hat{x}^2 \right\rangle\right) - \eta P_A. \tag{11b}$$

The system (10) and (11) is autonomous and also non-linear due to the quantum-classical interaction produced by $e_q^{cl} A^2 \hat{x}^2$ in (1). One also considers here the classical counterpart of the Hamiltonian (1)

$$H = \frac{1}{2}\left(\omega_q\left(x^2 + p^2\right) + \omega_{cl}\left(A^2 + P_A^2\right) + e_q^{cl} A^2 x^2\right). \tag{12}$$

Natural classical variables are (x, p, A, P_A). However, they are not convenient for our present purposes. We have to study the classical limit of (10) + (11). The comparison appeals to Poincare sections. Thus, we consider as classical variables $(x^2, p^2, L = 2xp)$ together with A, P_A. Via Hamilton's equations we obtain

$$\frac{dx^2}{dt} = \omega_q L, \tag{13a}$$

$$\frac{dp^2}{dt} = -\left(\omega_q + e_q^{cl} A^2\right) L, \tag{13b}$$

$$\frac{dL}{dt} = 2\left(\omega_q p^2 - \left(\omega_q + e_q^{cl}, A^2\right) x^2\right), \tag{13c}$$

$$\frac{dA}{dt} = \omega_{cl} P_A, \tag{13d}$$

$$\frac{dP_A}{dt} = -A\left(\omega_{cl} + e_q^{cl} x^2\right) - \eta P_A, \tag{13e}$$

which is a non linear system. Note in Eqs. (13a) and (13b) that L makes the system (13) an autonomous one.
We define I as

$$I = \langle \hat{x}^2 \rangle \langle \hat{p}^2 \rangle - \frac{\langle \hat{L} \rangle^2}{4} \geq \frac{\hbar^2}{4}, \tag{14}$$

a suitable motion-invariant for our system (10)-(11) in both regimens (conservative and dissipative) (see Appendix B). I is related to the uncertainty principle and describes deviation with respect to classicity, a condition characterized by $I = x^2 p^2 - L^2/4 = 0$ (trivial motion-invariant).
Eqs. (10) do not explicitly depend upon $\hbar$ while mean values depend on it via the initial conditions through I. The inequality (14) and its classical value, are crucial in our study of the classical limit $I \to 0$, as will be seen throughout the article. Focus now attention upon the relative energy E_r.

$$E_r = \frac{|E|}{I^{1/2}\omega_q}, \tag{15}$$

where $E = \langle H \rangle$ is the total energy. E_r is also a motion invariant that verifies $E_r \geq 1$ (due to the uncertainty principle). E_r is dimensionless. The LC is $I \to 0$, i.e.,

$$E_r \to \infty. \tag{16}$$

In the dissipative case we replace, in (15), E by $E(0)$ (see below). Our system of equations requires numerical treatment. Our main interest lies in the evolution of observables when E_r grows from its minimum unity value,

III. RESULTS

A. Conservative evolution

The systems (10)-(11) (semi classic) and (13) (classic) contain five equations each. There are two motion invariants (total energy E and I). Three independent variables remain. One can then construct Poincare sections. Here we work to such an effect with the plane $A = 0$. In our calculations we used an ample set of both parameters and initial conditions. We will present plots in which the independent variable is E_r. We fix the values $E = 0.6$ and $\omega_q = 1$. What we vary is just I. The ensuing results are compared to those of Refs. 15, 19–21. Additionally, our graphs correspond to $\omega_{cl} = e_q^{cl} = 1$. The independent initial conditions are, in the semi classic instance, $\langle \hat{L} \rangle(0)$, $\langle \hat{x}^2 \rangle(0)$, and $A(0)$. For the classic situation they are $L(0)$, $x^2(0)$, and $A(0)$.
We let $\langle \hat{x}^2 \rangle(0)$ to vary in the interval

$$\left(E/\omega_q - \sqrt{(E/\omega_q)^2 - I_L}, (0, E/\omega_q + \sqrt{(E/\omega_q)^2 - I_L}\right),$$

where $I_L = I + \langle L \rangle(0)^2/4$. This expression can be simplified by fixing $\langle L \rangle(0) = 0$ (with $I \leq (E/\omega_q)^2$), allowing the system to reach its ground state). For the classic variables we fix $L(0) = 0$ and permit $x^2(0)$ to move in the interval $(0, 2E/\omega_q)$. By appeal to (14) we see that $\langle \hat{p}^2 \rangle(0) = \dfrac{I}{\langle \hat{x}^2 \rangle}(0)$ ($p^2 = 0$ in the classical instance.) In addition, from (1) we deduce $P_A(0)$ via

$$P_A = \frac{\pm}{\omega_{cl}^{1/2}} \sqrt{2E - \omega_q(\langle \hat{p}^2 \rangle + \langle \hat{x}^2 \rangle) - e_q^{cl} A^2 \langle \hat{x}^2 \rangle - \omega_{cl} A^2},$$

evaluating all quantities at the initial time. We have also an equivalent classic version. Finally, we consider $A(0) = 0$ in both semi quantum and classic cases. In our calculations we have used a very wide range of values of E_r (or I). Our graphs illustrate the results that have been obtained. All simulations use Fortran and Phyton.

Figs. 1 depict, for the conservative scenario ($\eta = 0$), Poincare sections $\langle \hat{p}^2 \rangle$ versus $\langle \hat{x}^2 \rangle$. The following I values are considered: $I = 0.34999, 0.17499, 0.14999, 0.11249, 56.25 \times 10^{-4}, 6.12422 \times 10^{-4}, 3.6 \times 10^{-19}, 0$, for which $E_r = 1.01419, 1.143431, 1.54924, 1.78893, 2.52982, 24.2452, 10^9$, and also ∞. Note the absence of chaos. Secondly, sub-Figs. f) and g) display convergence to sub-Fig. h). sub-Fig. h) represents the pertinent classical Poincare section (for the associated classical system), see (13). The quantum-classical transition exhibits two zones: a first semi-quantum region (SC) and a second, classical, one that stars at approximately $E_r = 24.2452$ (sub-Fig. f). After this point convergence to the classic counterpart begins. The SC zone can be thought of as composed of two sub-zones. A cuasi-quantal $E_r \sim 1$ ($E_r = 1$ signals pure quantum behavior) and a transition regime from $E_r \sim 1$ to $E_r = 24.2452$. These sub-zones are represented by sub-Figs a)-b) and sub-Figs c)-d) respectively.

This sort of division has previously been encountered for another Hamiltonian, investigated in Refs. 15, 19–21. The

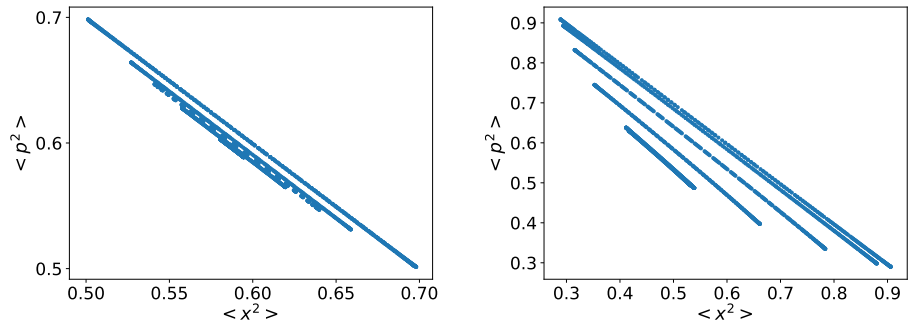

(a)$E_r = 1.01419$

(b)$E_r = 1.17109$

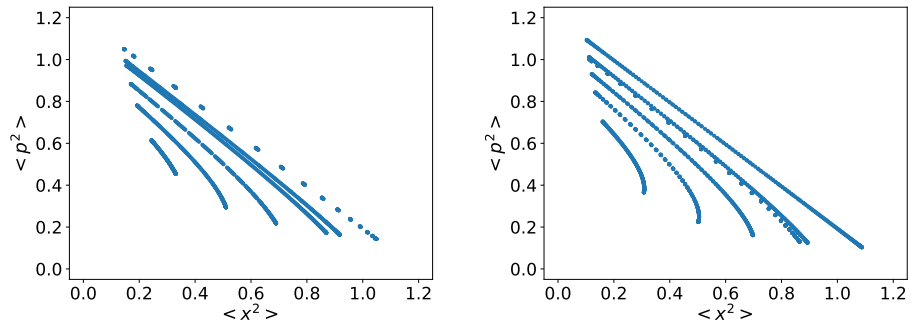

(c)$E_r = 1.54924$

(d)$E_r = 1.78893$

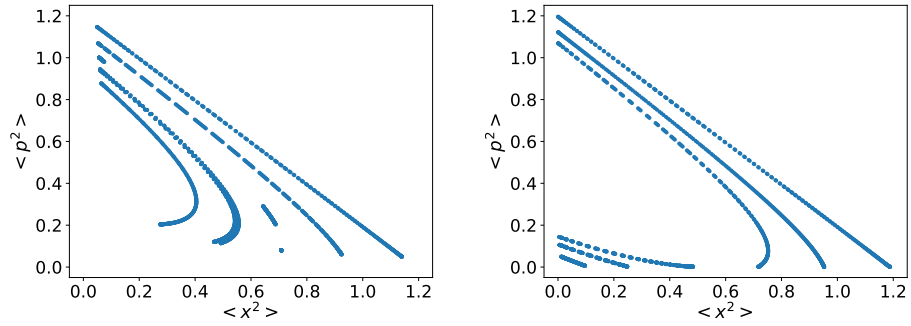

(e)$E_r = 2.52982$

(f)$E_r = 24.2452$

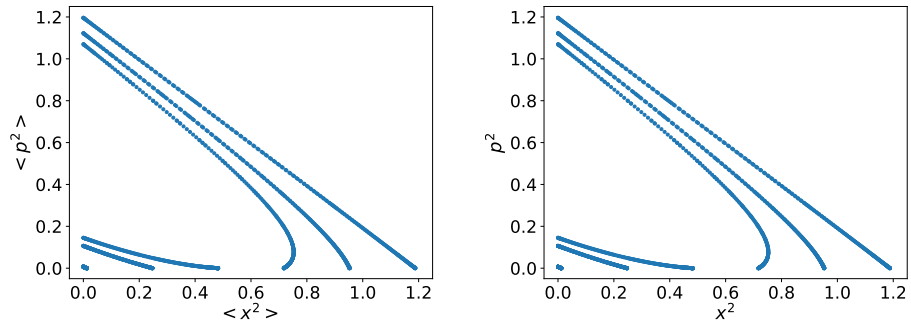

(g)$E_r = 10^9$

(h)$E_r \to \infty$.

FIG. 1. Poincare Sections with $A = 0$. We plot $\langle \hat{x}^2 \rangle$ vs $\langle \hat{p}^2 \rangle$. We can observe the convergence to the fully classical Sections (sub-Fig. h). In particular, note the similitude of sub-Figs. g) and h).

convergence there begins for the same E_r value of 24.2452 ($E_r = E_r{}^{cl}$)[19–21]. Note that with this other Hamiltonian one detects chaos, while here one does not. Note also that in Figs. 1) one always has

$$\langle \hat{x}^2 \rangle \langle \hat{p}^2 \rangle \geq I, \tag{17}$$

in compliance with the uncertainty principle (see (14)). For $I = 0$ the hyperbole $\langle \hat{x}^2 \rangle \langle \hat{p}^2 \rangle = I$ degenerates to the coordinate axes $\langle \hat{x}^2 \rangle = 0$ and $\langle \hat{p}^2 \rangle = 0$.

B. Dissipative evolution

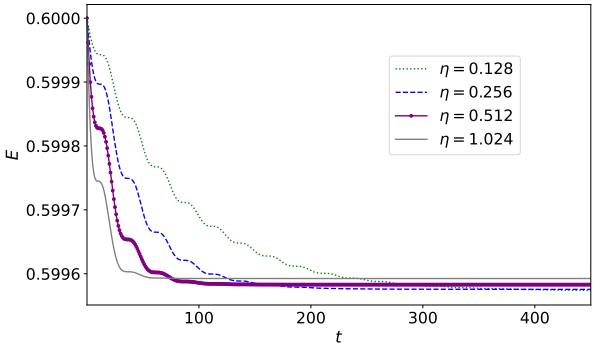

FIG. 2. We plot the total energy of the system $E = \langle \hat{H} \rangle$ vs. t, for several values of η. We take $E_r = 1.0142$.

We consider now, in Eqs. 11b) and 13e) the case $\eta > 0$. The dissipation process can be attributed to an interaction with a macroscopic system like a measurement instrument or with a thermal bath for which the classical variables A and P_A make sense. Note that the total energy E is no longer constant but decreases till an asymptotic, final value E_f at $t \to \infty$ [see Eq. (7)]. E_f must to be calculated numerically and coincides with E_{qf}, the asymptotic value of the quantum energy

$$E_q = \frac{\omega_q}{2}(\langle \hat{x}^2 \rangle + \langle \hat{p}^2 \rangle). \tag{18}$$

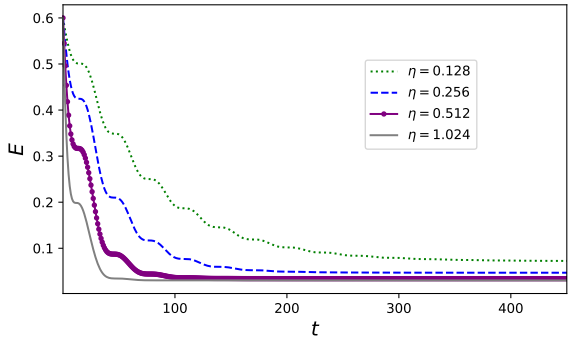

FIG. 3. We display the total energy E vs. t, for the values of η as in Fig. 2. We take now $E_r = 24.2452$.

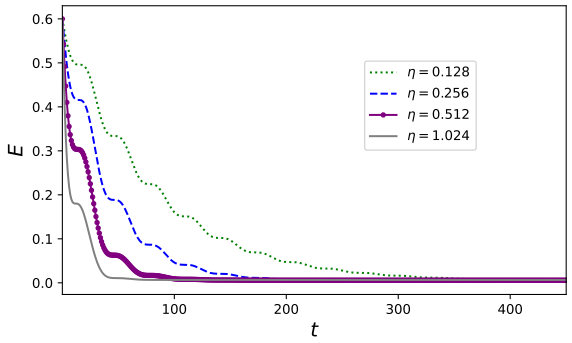

FIG. 4. E versus time for the values of η as in Fig. 2. We take now $E_r = 10^9$.

It is verified that $E_f = E_{qf} \geq I^{1/2}\,\omega_q$ due to the uncertainty principle.

For the classic counterpart we have $E_f \geq 0$. Instances $E_f = I^{1/2}\,\omega_q$ and $E_f = 0$ correspond to the single Fixed Point of our two systems, semi classic and classic respectively. For $E_f > I^{1/2}\,\omega_q$ and $E_f > 0$ we obtain the concomitant limit cycles (see below).

Figs. 2), 3), 4) on the one hand, and 5), 6), 7) on the other, represent, respectively, E and E_q vs. time, for different values of η and E_r. In the dissipative cases we redefine E_r as

$$E_r = \frac{|E(0)|}{I^{1/2}\omega_q}, \tag{19}$$

a function of the initial energy. The classical limit is $E_r \to \infty$. This definition obviously includes (15), when the system is conservative.

Note in Figs. 2), 3) and 4) that the rate of converge to $E_f = E_{qf}$ accelerates as η grows. Also, E_f diminishes as E_r grows. Figs. 4) y 7) are similar to their purely classic counterparts. In Figs. 5), 6) and 7), see that the curves are not monotonically decreasing, but $E_{qf} < E(0)$. It can also be seen that in Fig. 6) there is a change in concavity as $t \to \infty$. The E_q-curves are concave, contrary to what happens in Figs. 5) and 7). This figure corresponds to $E_r = 24.2452$, the approximate value of E_r from which, in the conservative regime, the convergence to the classical result begins.

1. *Fixed points, limit cycles, and stability analysis*

Fixed points (FP) are determined by the vanishing of the time derivatives in (10)-(11) (semi classic) and (13) (classic counterpart). For the semiclassical system, the FP are:

$$\langle \hat{x}^2 \rangle = \langle \hat{p}^2 \rangle = \sqrt{I} \text{ and } \langle \hat{L} \rangle = A = P_A = 0. \tag{20}$$

For the purely classical system the PF are

$$x^2 = p^2 = L = A = P_A = 0. \tag{21}$$

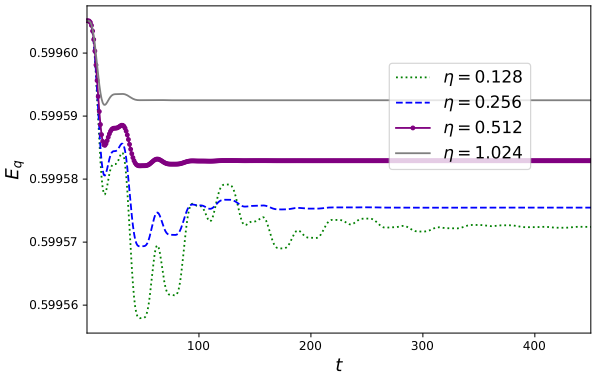

FIG. 5. E_q curves versus time for the same η-values as in Figs. 2), 3) and 4). We consider $E_r = 1.0142$.

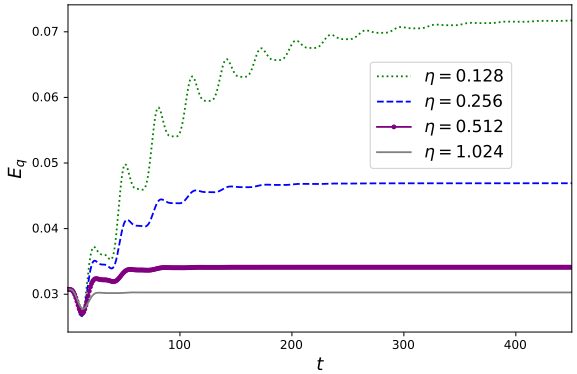

FIG. 6. E_q curves versus time for the same η-values and as in Figs. 2), 3) and 4). We consider $E_r = 24.2452$.

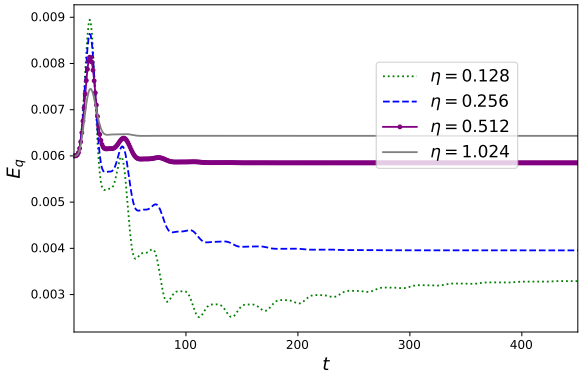

FIG. 7. E_q curves versus time for the same η-values as in Figs. 2), 3) and 4). We consider $E_r = 10^9$.

As for limit cycles (LC) we have in the semi classic instance

$$\langle \hat{x}^2 \rangle + \langle \hat{p}^2 \rangle = \frac{2E_f}{\omega_q}, \tag{22a}$$

$$\langle \hat{x}^2 \rangle \langle \hat{p}^2 \rangle = I + \frac{\langle \hat{L} \rangle^2}{4}. \tag{22b}$$

For the classic counterpart we obtain the LC evaluating the above system at $I = 0$. The LC corresponds to $E_f > I^{1/2}\,\omega_q$ ($E_f > 0$ for the classic counterpart). There is a continuum of Limit Cycles, obtained by changing $E(0)$ or I.

In a subspace generated by $\langle \hat{x}^2 \rangle, \langle \hat{p}^2 \rangle, \langle \hat{L} \rangle$, the cycles (22) are represented by special curves. Because of $\langle \hat{x}^2 \rangle$ and $\langle \hat{p}^2 \rangle$ are positive, these curves are determined by the intersection of the semi plane (22a) and the semi hyperboloid of two sheets with oblique axis (22b). In the classical case the semi hyperboloid reduces to a semi cone with the same symmetries. In both instances the LCs are unstable (or marginally unstable). Keeping $E(0) = E_f$ - I fixed and slightly altering any initial condition, without staying on the cycle, the ensuing evolution lead to another LC with the same I and a slight change in E_f. The FP (20) and (21) can be seen as extreme degenerate situations of the LC for E_f reaching its minimum values $E_f = I^{1/2}\,\omega_q$ and $E_f = 0$. They are unstable for the same reasons invoked above. We can perform an analytical study consistent with these results, using the Jacobian matrix evaluated in the FPs, which becomes

$$\begin{pmatrix} 0 & 0 & \omega_q & 0 & 0 \\ 0 & 0 & -\omega_q & 0 & 0 \\ -2\omega_q & 2\omega_q & 0 & 0 & 0 \\ 0 & 0 & 0 & 0 & \omega_{cl} \\ 0 & 0 & 0 & -\omega_{cl} - e_q^{cl}\sqrt{I} & -\eta \end{pmatrix}. \tag{23}$$

The classical corresponding Jacobian matrix emerges setting $I = 0$ in (23). The pertinent eigenvalues are 0, $\pm 2|\omega_q|i$ and $-\eta/2 \pm \sqrt{-4\omega_{cl}^2 - 4\omega_{cl} e_q^{cl}\sqrt{I} + \eta^2}\,/2$. The null eigenvalue is associated to the presence of the invariant of motion I. Two eigenvalues are purely imaginary and the two remaining ones are negative or have a negative real part and an imaginary one (for $e_q^{cl} < -\omega_{cl}/\sqrt{I}$, which is verified in our case). The set indicates the tendency to a CL infinitesimally close to the considerate FP (for semiclassical or classical cases). Thus the Fixed Points are marginally unstable.

2. *Poincare sections and Projections*

We deal now with four independent variables since the total energy is not conserved any longer. To obtain Poincare sections we need to intersect the solutions of our system of equations with two planes. We intersect with $A = 0$ which yields three dimensions (3D) sections. Then we project them onto the subspace determined by a pair of mean values of the set $(\hat{x}^2, \hat{p}^2, \hat{L} = \hat{x}\hat{p} + \hat{x}\hat{p})$. We fix $E(0) = 0.6$ and also use the remaining initial conditions of the conservative evolution.

As in the conservative case, in our calculations we employ a very wide range of values of E_r (or I). In Figs. 8) we plot

representative 3D sections with $A = 0$, varying E_r as in Figs. 1). We clearly observe the LC given by Eqs. (22) and also isolated points satisfying $A = 0$. The cycles are planar curves on the semi hyperboloid cited above. We do not plot the FP corresponding to the hyperboloid vertex. As E_r grows, the hyperboloid's curvature diminishes. It converges to a semi cone corresponding to the purely classic Hamiltonian. This convergence takes place approximately for $E_r = 24.2452$, corresponding to sub-Fig. f). After that E_r-value, it is hard to distinguish between the 3D Sections. For example between sub-Figs. g) and sub-h) (classic for $I = 0$, $E_r \to \infty$). This $E_r = 24.2452$ value coincides with that detected for the conservative case and a different scenario in Kowalski et al (Ref. 15).

Figs. 9) depict projections of the 3D Sections discussed in Figs. 8) onto the sub-space $(\langle \hat{x}^2 \rangle, \langle \hat{p}^2 \rangle)$. The convergence begins approximately at $E_r = 24.2452$ in sub-Fig. f), i.e. this E_r value signals the limit between semi classic and totally classic zones as in the conservative regime. In this case also the semi classical zone can be regarded as consisting of two subregions, a quasi quantum $E_r \sim 1$ and a transition regime from $E_r \sim 1$ to $E_r = 24.2452$. In Figs. 9, inequality (17) is obeyed as well.

IV. CONCLUSIONS

In this work we analyzed the dynamics of the bipartite semi classic Hamiltonian (1) together with the associated classical limit (CL). We studied both conservative and dissipative time-evolutions using Eqs. (2), (3), and (5). The CL was investigated using a parameter E_r defined in (15) for the conservative instance and in (19) for the dissipative one. We have focused attention upon Poincare sections (PS). They arise from the intersection with the plane $A = 0$. In the conservative situation we have 2D PS (Figs. 1). In the dissipative one, we have 3D PS (Figs. 8). We also used the PS projections onto the sub-space $(\langle \hat{x}^2 \rangle, \langle \hat{p}^2 \rangle)$ in the last case (Figs. 9). We studied as well time evolutions for the total and quantal energy (Figs. 2-7). We ascertain that the final energy $E_f = E_{qf}$ diminishes as E_r grows.

Our semi classic results are clearly seen to converge to the totally classic ones ($I = 0$). Our graphs (for instance, Figs. 1), 8) y 9)) distinguish two zones. A semi quantum one and a semi classic region. They are separated by a special E_r-value $E_D = 24.2452$. Approximately for $E_r \sim E_D$ our computed values start to converge to the classical ones. This happens for both the dissipative and conservative regimes. Surprisingly, E_D coincides with for that particular value obtained with the same methodology for another Hamiltonian studied in Refs. 15, 19–21. In our present model, no chaos was found. In the just referred to model, chaos does arise. Also notice the change of curvature in the quantal energy curves at the same E_r value (Fig. 6). Finally, we observe in Figs. 1) and 9) compliance with the Uncertainty Principle.

ACKNOWLEDGMENTS

A. M. K. and G. G. acknowledge support from the Comisión de Investigaciones Científicas de la Provincia de Buenos Aires (CICPBA) of Argentina. A. P. acknowledges support from Universidad Nacional de La Plata.

Appendix A: Demonstration of equation (9)

We first prove Eq. (9), for a general semiclassical hamiltonian $\hat{H}$ with an interaction $\hat{H}\left(A,\hat{O}\right)$ constrained to not to depend on P_A (so that the assocciated calculations become less cumbersome).

$$\hat{H} = \hat{H}_q + H_{cl}\hat{I} + \hat{H}\left(A,\hat{O}\right) \to \langle \hat{H} \rangle = \langle \hat{H}_q \rangle + H_{cl}\langle \hat{I} \rangle + \langle \hat{H}\left(A,\hat{O}\right) \rangle. \tag{A1}$$

We also consider the classical Hamiltonian (8) and use Eqs. (5). We wish to reach (9).

$$\begin{aligned}
\frac{d}{dt}\langle \hat{H} \rangle &= \frac{d}{dt}\langle \hat{H}_q \rangle + \frac{d}{dt}\langle \hat{H}\left(A,\hat{O}\right) \rangle + \frac{d}{dt}\langle H_{cl} \rangle \\
&= \langle \left[\hat{H}\left(A,\hat{O}\right),\hat{H}_q\right] \rangle + \langle \left[\hat{H}_q,\hat{H}\left(A,\hat{O}\right)\right] \rangle + \frac{\partial \langle \hat{H}\left(A,\hat{O}\right) \rangle}{\partial A}\frac{dA}{dt} + \frac{dH_{cl}}{dt} = \frac{\partial \langle \hat{H}\left(A,\hat{O}\right) \rangle}{\partial A}\frac{dA}{dt} + \frac{dH_{cl}}{dt} \\
&= \frac{\partial \langle \hat{H}\left(A,\hat{O}\right) \rangle}{\partial A}\frac{P_A}{M} + \frac{dH_{cl}}{dt} = \frac{\partial \langle \hat{H}\left(A,\hat{O}\right) \rangle}{\partial A}\frac{P_A}{M} + \frac{P_A}{M}\frac{dP_A}{dt} + \frac{\partial V}{\partial A}\frac{P_A}{M} \\
&= \frac{\partial \langle \hat{H}\left(A,\hat{O}\right) \rangle}{\partial A}\frac{P_A}{M} + \frac{P_A}{M}\left(-\frac{\partial V}{\partial A} - \frac{\partial \langle \hat{H}\left(A,\hat{O}\right) \rangle}{\partial A} - \eta P_A\right) + \frac{\partial V}{\partial A}\frac{P_A}{M} \\
&= -\frac{\eta}{M}P_A^2.
\end{aligned}$$

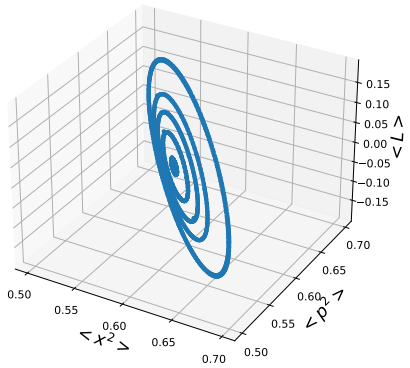

(a)$E_{r_0} = 1.01419$

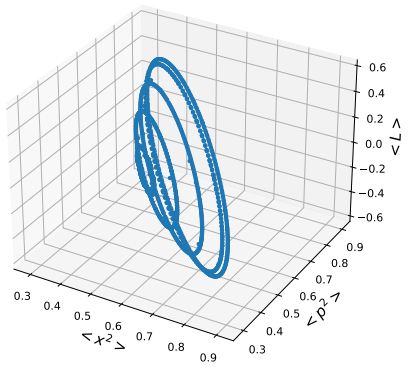

(b)$E_r = 1.17109$

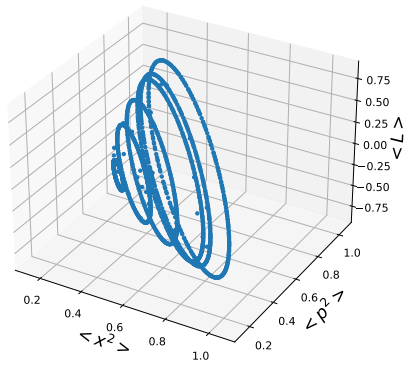

(c)$E_r = 1.54924$

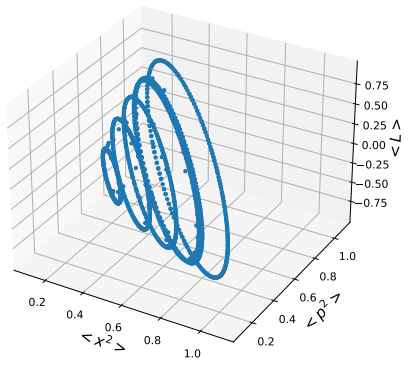

(d)$E_r = 1.78893$

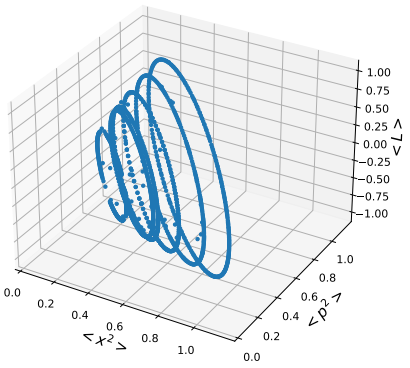

(e)$E_r = 2.52982$

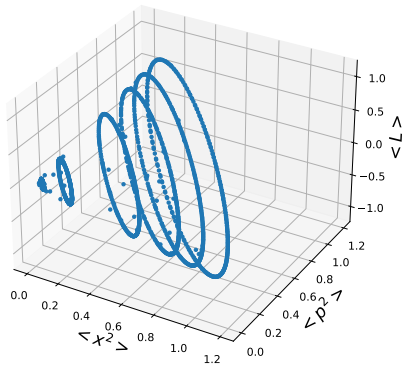

(f)$E_r = 24.2452$

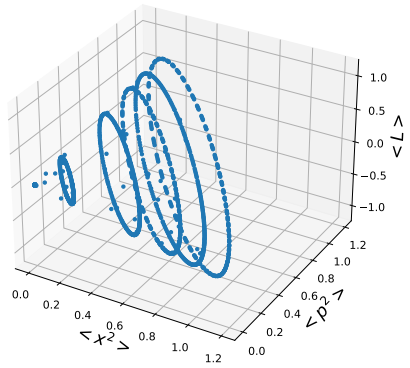

(g)$E_r = 10^9$

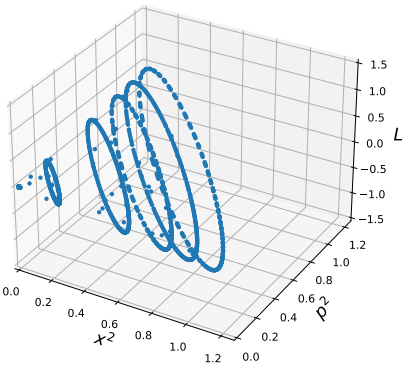

(h)$E_r = \infty$

FIG. 8. Dissipative system. 3D Poincare sections for $A = 0$ corresponding to $\langle \hat{x}^2 \rangle$, $\langle \hat{p}^2 \rangle$, and $\langle \hat{L} \rangle$. Initial conditions are the same as in the conservative regime. We take $\eta = 0.05$. See the convergence towards sub-Fig. h) and the similitude between sub-Figs. g) and h).

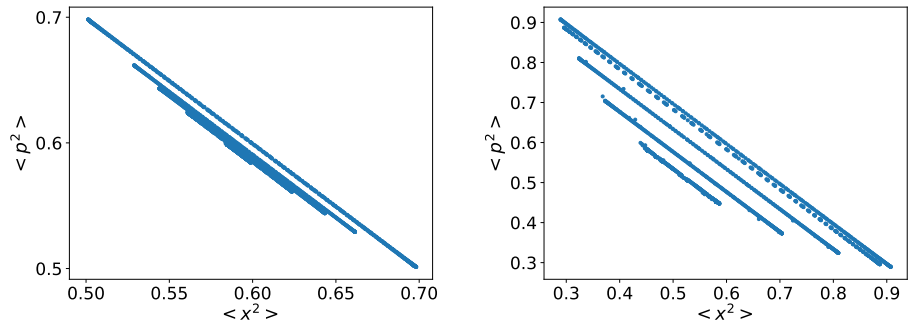

(a)$E_r = 1.01419$

(b)$E_r = 1.17109$

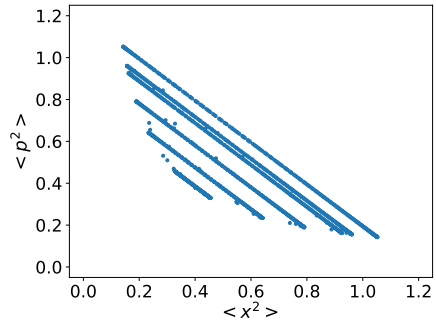

(c)$E_r = 1.54924$

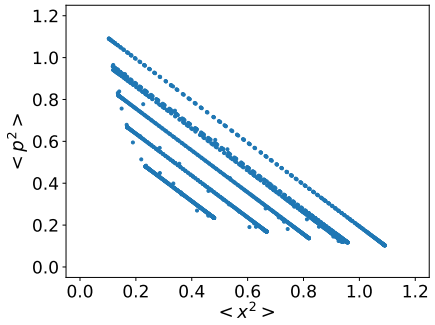

(d)$E_r = 1.78893$

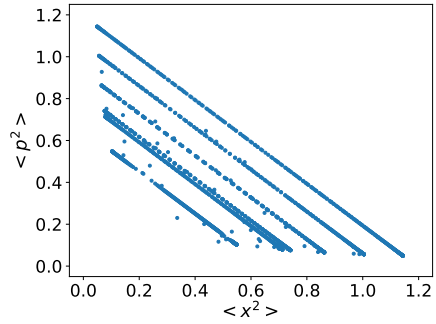

(e)$E_r = 2.52982$

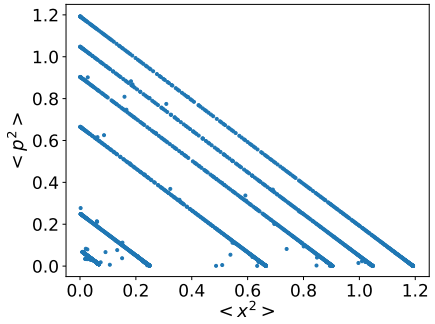

(f)$E_r = 24.2452$

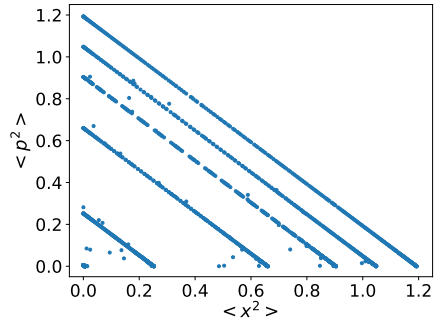

(g)$E_r = 10^9$

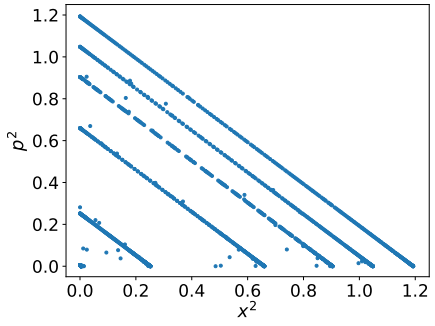

(h)$E_r = \infty$

FIG. 9. Projections of the 3D Poincare sections of the Fig. 8) on the subspace $\langle \hat{x}^2 \rangle$- $\langle \hat{p}^2 \rangle$. See the convergence toward la sub-Fig. h). In particular the similarity of sub Figs. g) and h).

Recall that $\hat{I}$ is the identity operator. The last line above coincides with dH_{cl}/dt. A better visualization arise from Eq. (9) adapted to the particular form of the Hamiltonian (1):

$$\begin{aligned}
\langle \hat{H} \rangle &= \frac{1}{2}\left(\omega_q\left(\langle \hat{x}^2\rangle + \langle \hat{p}^2\rangle\right) + \omega_{cl}\left(A^2 + P_A^2\right)\langle \hat{I}\rangle + e_q^{cl}A^2\langle \hat{x}^2\rangle\right) \\
\frac{d\langle \hat{H}\rangle}{dt} &= \frac{1}{2}\left[\omega_q\left(\frac{d}{dt}\langle \hat{x}^2\rangle + \frac{d}{dt}\langle \hat{p}^2\rangle\right) + \omega_{cl}\left(\frac{d}{dt}A^2 + \frac{d}{dt}P_A^2\right) + e_q^{cl}\frac{d}{dt}A^2\langle \hat{x}^2\rangle\right] \\
&= \frac{1}{2}\left[\omega_q\left(\frac{d\langle \hat{x}^2\rangle}{dt} + \frac{d\langle \hat{p}^2\rangle}{dt}\right) + \omega_{cl}\left(2A\frac{dA}{dt} + 2P_A\frac{dP_A}{dt}\right) + e_q^{cl}2A\frac{dA}{dt}\langle \hat{x}^2\rangle + e_q^{cl}A^2\frac{d\langle \hat{x}^2\rangle}{dt}\right] \\
&= \frac{1}{2}\left[\omega_q\left(\omega_q\langle \hat{L}\rangle - \omega_q\langle \hat{L}\rangle - e_q^{cl}A^2\langle \hat{L}\rangle\right) + \omega_{cl}\left(2\omega_{cl}AP_A + 2P_A\left(-\omega_{cl}A - e_q^{cl}A\langle \hat{x^2}\rangle - \eta P_A\right)\right) + 2\omega_{cl}e_q^{cl}AP_A\langle \hat{x}^2\rangle + \omega_q e_q^{cl}A^2\langle \hat{L}\rangle\right] \\
&= -\omega_{cl}\eta P_A^2
\end{aligned}$$

Appendix B: I as invariant of motion

We consider a semiclassical Hamiltonian. It is fully general in classical variables. It has a general quadratic form in quantum operators.

$$\hat{H} = \frac{1}{2}\left(\alpha\hat{p}^2 + s\beta\hat{x}^2 + H_{cl}\hat{I} + \gamma C_{cl}\hat{x}^2\right), \tag{B1}$$

where s can take the following values, $s = 1, 0, -1$, representing a harmonic oscillator, a free particle, or a particle in an inverse parabolic potential, respectively (we take $\alpha > 0, \beta > 0$). We also consider the classical Hamiltonian Hcl of (8). Additionally C_{cl} is a general function of the classical variables $C_{cl} = C(A, P_A)$. We derive now the quantity I defined in equation (14) with respect to time

$$\frac{dI}{dt} = \frac{d\langle \hat{x}^2\rangle}{dt}\langle \hat{p}^2\rangle + \langle \hat{x}^2\rangle\frac{d\langle \hat{p}^2\rangle}{dt} - \frac{2}{4}\langle \hat{L}\rangle\frac{d\langle \hat{L}\rangle}{dt}.$$

We need the derivatives of the set $(\hat{x}^2, \hat{p}^2, \hat{L})$, which are obtained using Eqs. (3) and (B1)

$$\frac{d\langle \hat{x}^2\rangle}{dt} = \alpha\langle \hat{L}\rangle, \tag{B2a}$$

$$\frac{d\langle \hat{p}^2\rangle}{dt} = -\left(s\beta + \gamma C_{cl}\right)\langle \hat{L}\rangle, \tag{B2b}$$

$$\frac{d\langle \hat{L}\rangle}{dt} = 2\left(\alpha\langle \hat{p}^2\rangle - \left(s\beta + \gamma C_{cl}\right)\langle \hat{x}^2\rangle\right), \tag{B2c}$$

Then

$$\begin{aligned}
\frac{dI}{dt} &= \alpha\langle \hat{L}\rangle\langle \hat{p}^2\rangle - \langle \hat{x}^2\rangle\left(s\beta + \gamma C_{cl}\right)\langle \hat{L}\rangle - \langle \hat{L}\rangle\left(\alpha\langle \hat{p}^2 - \left(s\beta + \gamma C_{cl}\right)\langle \hat{x}^2\rangle\right) \\
&= 0.
\end{aligned}$$

Thus, I is an invariant of motion. Note that although the system of equations (B2) contains the classical variables, its temporal evolution is not needed to prove that I is motion invariant. This is a property of an entirely of quantum origin.

[1] N. D. Birell and P. C. W. Davies, 2019, Semiclassical Physics, CRC Press

[2] Struyve, W. (2020). Semi-classical approximations based on Bohmian mechanics. International Journal of Modern Physics A, 35(14), 2050070.

[3] Joos, E., Zeh, H. D., Kiefer, C., Giulini, D. J., Kupsch, J., & Stamatescu, I. O. (2013). Decoherence and the appearance of a classical world in quantum theory. Springer Science & Business Media.

[4] Arndt, M., Hornberger, K., & Zeilinger, A. (2005). Probing the limits of the quantum world. Physics world, 18(3), 35.

[5] Zeh, H. D. (1999). Why Bohm's quantum theory?. Foundations of Physics Letters, 12(2), 197-200.

[6] Bloch, F. (1946). Nuclear induction. Physical review, 70(7-8), 460.

[7] Milonni, P. W., Shih, M. L., & Ackerhalt, J. R. (1987). Chaos in laser-matter interactions (Vol. 6). World Scientific Publishing Company.

[8] Ring, P., & Schuck, P. (2004). The nuclear many-body problem. Springer Science & Business Media.

[9] Ribeiro, R. F., & Burke, K. (2018). Deriving uniform semiclassical approximations for one-dimensional fermionic systems. The Journal of Chemical Physics, 148(19), 194103.

[10] D'Alessio, L., Kafri, Y., Polkovnikov, A., & Rigol, M. (2016). From quantum chaos and eigenstate thermalization to statistical mechanics and ther-

modynamics. Advances in Physics, 65(3), 239-362.
[11]Gravielle, M. S., & Miraglia, J. E. (2014). Semiquantum approach for fast atom diffraction: Solving the rainbow divergence. Physical Review A, 90(5), 052718.
[12]Barker, J., & Bauer, G. E. (2019). Semiquantum thermodynamics of complex ferrimagnets. Physical Review B, 100(14), 140401.
[13]Kowalski, A. M., & Rossignoli, R. (2018). Nonlinear dynamics of a semiquantum Hamiltonian in the vicinity of quantum unstable regimes. Chaos, Solitons & Fractals, 109, 140-145.
[14]Cooper, F., Dawson, J., Habib, S., & Ryne, R. D. (1998). Chaos in time-dependent variational approximations to quantum dynamics. Physical Review E, 57(2), 1489.
[15]Kowalski, A. M., Plastino, A., & Proto, A. N. (2002). Classical limits. Physics Letters A, 297(3-4), 162-172.
[16]Alhassid, Y., & Levine, R. D. (1978). Connection between the maximal entropy and the scattering theoretic analyses of collision processes. Physical Review A, 18(1), 89.
[17]Levine, R. D., Napoli, D. R., Otero, D., Plastino, A., & Proto, A. N. (1986). Maximum entropy approach to nuclear fission processes. Nuclear Physics A, 454(2), 338-358.
[18]Kowalski, A. M., Plastino, A., & Proto, A. N. (1995). Semiclassical model for quantum dissipation. Physical Review E, 52(1), 165.
[19]Kowalski, A. M., Plastino, A., & Proto, A. N. (1997). A semiclassical statistical model for quantum dissipation. Physica A: Statistical Mechanics and Its Applications, 236(3-4), 429-447.
[20]Kowalski, A.M.; Plastino, A., Asger S. Thorsen (Ed.). (2020), Semiquantum Time evolution. Classical limit. Nova.
[21]Kowalski, A. M., & Plastino, A. (2022). Classical-Quantum Transition as a Disorder-Order Process. Entropy, 24(1), 87.
[22]Arnol'd, V. I. (2013). Mathematical methods of classical mechanics (Vol. 60). Springer Science & Business Media.